

# Technical Note: Skirt-chamber – an open dynamic method for the rapid and minimally-intrusive measurement of greenhouse gas emissions from peatlands

5 Frederic Thalasso<sup>1,2</sup>, Brenda Riquelme<sup>2,3</sup>, Andrés Gómez<sup>2</sup>, Roy Mackenzie<sup>2,3</sup>, Francisco Javier Aguirre<sup>2</sup>, Jorge Hoyos-Santillan<sup>2,4,5</sup>, Ricardo Rozzi<sup>2</sup>, Armando Sepulveda-Jauregui<sup>2,4,5</sup>

<sup>1</sup>Departamento de Biotecnología y Bioingeniería, Centro de Investigación y de Estudios Avanzados del Instituto Politécnico Nacional (Cinvestav), Mexico City, 07360, Mexico

10 <sup>2</sup>Cape Horn International Center, Universidad de Magallanes, Puerto Williams, 6350000, Chile

<sup>3</sup>Millennium Institute Biodiversity of Antarctic and Subantarctic Ecosystems (BASE), Santiago, 7800003, Chile

<sup>4</sup>Environmental Biogeochemistry Laboratory, Centro de Investigación Gaia Antártica (CIGA), Universidad de Magallanes, Punta Arenas, 6210427, Chile

<sup>5</sup>Center for Climate and Resilience Research (CR)2, Universidad de Chile, Santiago, 7800003, Chile

15 *Correspondence to:* F. Thalasso (thalasso@cinvestav.mx); A. Sepulveda-Jauregui (armando.sepulveda@umag.cl)

**Abstract.** We present a reliable and robust open dynamic chamber for measuring greenhouse gas exchange in peatlands with minimal disturbance of the ground. This chamber, called “skirt-chamber”, is based on a transparent plastic film, placed above an open frame made of sparse interwoven wires, and expanded around the base of the chamber below a steel chain that ensures contact to the ground, avoiding damage, trenching or cutting vegetation. Gas exchange is determined using a portable gas analyser from a mass balance in which the imperfect sealing of the chamber to the ground is quantified through the injection a methane pulse. The method was tested on a pristine peatland dominated by *Sphagnum magellanicum* located on Navarino Island at the subantarctic Magellanic ecoregion in Chile. Our results indicate that, the skirt-chamber allowed determining methane fluxes and ecosystem respiration, in about 20 minutes, with a limit of detection of 0.185 mg CH<sub>4</sub> m<sup>-2</sup> h<sup>-1</sup>, and 173 mg CO<sub>2</sub> m<sup>-2</sup> h<sup>-1</sup>, respectively. We conclude that the skirt-chamber is a minimally-intrusive, fast, portable, and inexpensive method that allows the quantification of greenhouse gas emissions with high spatial resolution in remote locations and without delay.

## 1 Introduction

Peatlands are a major component of the global carbon cycle and are the largest carbon reservoir in the biosphere (Yu et al., 2011). These ecosystems hold  $\approx 644$  gigatons of carbon (GtC) in 399 million ha (Leifeld and Menichetti, 2018). For that reason, peatlands have gained relevance as potential Nature-based Solution (NbS) to help addressing global warming (Griscom et al., 2017; UNEP, 2019). At present, peatlands act globally as carbon sinks, sequestering 0.1 GtC y<sup>-1</sup> (Frolking et al., 2011). However, peatlands are also among the largest greenhouse gas emitters to the atmosphere (IPCC, 2021), including carbon dioxide (CO<sub>2</sub>) as product of the ecosystem respiration and methane (CH<sub>4</sub>) produced through anaerobic processes. Consequently, peatlands can behave as carbon sink or net sources through time at different time scales (e.g., diurnal, seasonal,

decadal, millennial) and spatial scales (i.e., site, watershed, region) (Ding et al., 2004; Günther et al., 2014; Cobb et al., 2017; Swails et al., 2021). The shift from sink to net source, or vice versa, depends on different factors (e.g., climatic conditions, hydrology, anthropogenic impacts) (Leifeld and Menichetti, 2018; Günther et al., 2020; Page et al., 2022). Thus, under the current context of global climate change and accelerated land use change, it is important to accurately assess whether peatlands behave as carbon sinks or net sources and for that reason it is necessary to improve the temporal and spatial resolution when measuring greenhouse gas emissions in these ecosystems (Lawson et al., 2014).

In peatlands, greenhouse gas exchanges with the atmosphere are currently determined using above-ground and ground-based methods. Above-ground methods are mostly based on the eddy covariance (EC) techniques (Aubinet et al., 2012). Ground based methods consist of chambers placed on the surface of the terrain, which allow to quantify greenhouse gas fluxes at specific locations of the ecosystem. Ground based methods involve either a discrete sampling and measurement of the chamber's headspace, or a continuous monitoring of the chamber's headspace with a gas analyzer. The use of automatic chambers, that open and close at predetermined intervals, has allowed increasing the temporal resolution (Pavelka et al., 2018). However, chamber methods also present several drawbacks; for example, the increase or decrease of the gas concentration within the chamber headspace has a direct impact on the concentration gradient between the ground and the chamber headspace, ultimately altering the flux (Kutzbach et al., 2007; Juszczak, 2013; Pirk et al., 2015; Limpert et al., 2020). Another potential drawback is that the chambers sometimes do not include a fan to homogenize the air, causing local gradients, which modify the measured fluxes, underestimating them by at least one-third (Christiansen et al., 2011; Juszczak, 2013; Pavelka et al., 2018). More importantly, chambers require to be well sealed to avoid gas exchange between the atmosphere and the chamber headspace. To avoid leakiness, chambers are usually installed on a collar that drives several centimeters into the ground, sometimes combined with a water-filled groove.

The use of collars presents additional drawbacks, especially in peatlands characterized by uneven terrain and a dense vegetation rug. First, the collar installation implies some disturbance of the ecosystem, such as cutting the vegetation around the collar to allow its penetration into the ground. This procedure creates a trenching effect that must be considered in measurement protocols (Järveoja et al., 2020). Thus, after collar installation, it is a common practice to wait between 24 to 48 h before starting flux measurements. A collateral impact of the collar strategy is that, due to the delay in measurement, it significantly limits the number of locations where flux can be measured in each experimental timeframe, thus limiting both the temporal and spatial resolution of the studies, particularly in remote areas. Second, chamber installation would generally be preferred in relatively flat and even terrain over sloped or uneven ground, thus involving a bias selection of the locations where fluxes are measured. Third, automatic chambers are relatively expensive, thus most of the studies involving them use a few simultaneous chambers operated over days to weeks. This strategy offers an excellent temporal resolution but a relatively poor spatial resolution that could potentially lead to pseudoreplication, i.e. replicates not statistically independent.

To elude the former drawbacks, half a century ago, Edwards and Sollins (1973) suggested a new concept of chamber through which a known carrier gas flows continuously. The gas concentration is measured at the outlet of the chamber and the flux is determined after resolving a mass balance equation that involves all inputs and outputs of the chamber. According to the

Livingston and Hutchinson’s classification (Livingston and Hutchinson, 1995), that concept corresponds to a steady-state through-flow chamber, called “open dynamic chamber” (ODC), by opposition to standard static and dynamic chambers, which are non-steady-state chambers. The advantages of ODCs include a limited gas concentration buildup in the chamber and the continuous measurement of flux over the deployment time. More importantly, ODC measurements are not affected by leaks, as far as the carrier gas composition and flow is precisely known (see Section 2.1 for details). Thus, ODCs have the potential to elude the strict requirement of hermetic sealing and, therefore, to avoid disturbances and measurement delay caused by collar installation. Furthermore, the carrier gas of standard ODCs could be substituted by the natural air exchange caused by imperfect sealing of the chamber exposed to wind, as far as the flowrate of the air exchange is known. The substitution of a carrier gas for the quantification of the gas exchange with the environment would allow to avoid the use of heavy gas cylinders, advantageous for the rapid deployment of a simple, low-cost chamber able to quantify greenhouse gas emission or capture, by simply positioning the chamber on the surface of the peatland without penetration into the ground. This chamber could be then placed on any surface, independently of the vegetation cover, slope or terrain unevenness.

The objective of this study was to present the test concept of a modified ODC, called hereinafter the “skirt-chamber”, referring to the plastic skirt that is used to make contact with the ground. We tested the skirt-chamber design in the laboratory and in a peatland dominated by *Sphagnum magellanicum* on Navarino Island (Lat. 55°S), in the sub-Antarctic Magellanic ecoregion of Chile, characterized by an oceanic climate (Rozzi et al., 2012). Our research focused on evaluating the capacity of the skirt-chamber to measure CH<sub>4</sub> and CO<sub>2</sub> net emissions/capture, as well as the respiration rates of the ecosystem at different vegetation covers and terrain. In addition, one of our main goals was to develop a reliable and robust tool that was easy to operate and transport to remote areas, where data about the gas exchanges between peatlands and the atmosphere are limited.

## 2 Materials and methods

### 2.1. Skirt-chamber

The skirt-chamber (Fig. 1, details provided in Section 2.3) consists of an open frame made of sparse interwoven steel wires, whose purposes are supporting a transparent plastic film and defining the chamber’s volume while allowing light penetration. On top of the frame (installed on the ground, facing down), the plastic film is expanded over the frame and fixed at its base. When installing the chamber on the ground, the plastic film is expanded on the ground around the chamber and a steel chain is placed above it, surrounding three times the base of the chamber, to ensure that the plastic film is in contact with the ground. Thus, this design creates a fixed volume chamber, opened at the bottom and in contact with the ground. Inside the chamber, a fan is placed to homogenize the air content. Inlet and outlet ports are fixed on opposite sides of the frame and connected, in a recirculation mode, to a laser ultraportable greenhouse analyzer (*i.e.* UGGA, model 915-0011-1000, Los Gatos Inc., San Jose, CA, USA).

The gas mass balance of the skirt-chamber can be described by Equations 1–3;

$$\frac{dC_C}{dt} = inlets - outlets = flux + leak\ inlet - leak\ outlet \quad (1)$$

$$100 \quad \frac{dC_C}{dt} = F \cdot \frac{A_C}{V_C} + \frac{Q_L}{V_C} \cdot C_L - \frac{Q_L}{V_C} \cdot C_C \quad (2)$$

$$\frac{dC_C}{dt} = F \cdot \frac{A_C}{V_C} + \frac{Q_L}{V_C} \cdot (C_L - C_C) \quad (3)$$

Where  $C_C$  is the gas concentration inside the chamber ( $\text{mg m}^{-3}$ );  $F$  is the flux between the chamber and the ground ( $\text{mg m}^{-2} \text{h}^{-1}$ );  $A_C$  is the area of the chamber in contact with the ground ( $\text{m}^2$ );  $V_C$  is the chamber volume ( $\text{m}^3$ );  $Q_L$  is the flowrate of the gas exchange between the chamber and the exterior, caused by the imperfect seal between the chamber and the ground, ( $\text{m}^3 \text{h}^{-1}$ ); and,  $C_L$  is the gas concentration outside the chamber at ground level.

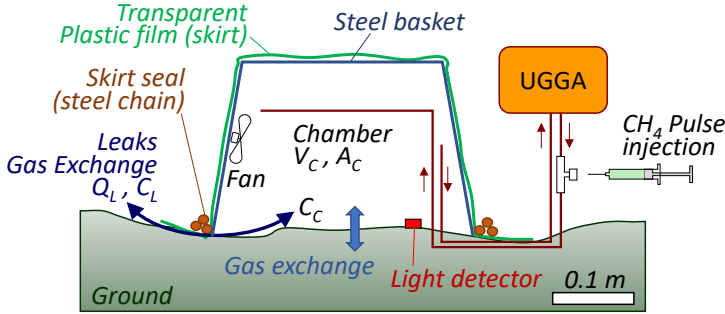


**Figure 1. Skirt-chamber concept (see text for details).**

The term  $Q_L/V_C$  is the dilution rate caused by the gas exchange between the chamber and the environment (Eqs. 2, 3), which is the inverse of the mean gas residence time in the chamber ( $\theta_C$ ), in such manner that Equation 3 becomes;

$$110 \quad \frac{dC_C}{dt} = F \cdot \frac{A_C}{V_C} + \frac{(C_L - C_C)}{\theta_C} \quad (4)$$

At equilibrium, *i.e.* concentration not changing over time,  $dC_C/dt$  equals zero, the concentration of the gas in the chamber can be considered as the constant  $C_B$  (baseline concentration). Under these conditions, Equation 4 becomes;

$$F = -\frac{(C_L - C_B)}{\theta_C} \cdot \frac{V_C}{A_C} = \frac{(C_B - C_L)}{\theta_C} \cdot \frac{V_C}{A_C} \quad (5)$$

Thus, as  $V_C$  and  $A_C$  are known,  $F$  can be determined during chamber deployment from the measurement of  $C_L$ ,  $C_B$ , and  $\theta_C$ .

115  $\theta_C$  can be determined in the field through the injection of a gas pulse within the chamber. Under these conditions, the steady-state is lost and by substitution of  $F$  (Eq. 5) in Equation 4, we obtain Equation 6;

$$\frac{dC_C}{dt} = -\frac{(C_L - C_B)}{\theta_C} \cdot \frac{V_C}{A_C} \cdot \frac{A_C}{V_C} + \frac{(C_L - C_C)}{\theta_C} = \frac{(C_B - C_C)}{\theta_C} \quad (6)$$

Since  $C_B$  is a constant, under fixed experimental conditions, Equation 6 can be rewritten as follows;

$$\frac{d(C_B - C_C)}{(C_B - C_C)} = -\frac{dt}{\theta_C} \quad (7)$$

120 And, after integration over time  $t$ , we obtain;

$$C_{C,t} = C_B + (C_{C,0} - C_B) \cdot e\left(-\frac{t}{\theta_C}\right) \quad (8)$$

Where  $C_{C,t}$  and  $C_{C,0}$  are the gas concentration within the chamber, at time  $t$  and shortly after the injection of a gas pulse, respectively. Equation 8 describes how, after a gas pulse has been injected,  $C_C$  return asymptotically to the equilibrium

concentration  $C_B$ . Thus, the injection of a gas pulse allows to determine  $\theta_C$ , which can be then used to estimate  $F$  by using  
125 Equation 5.

In these mass balance equations, it is important to stress that, during field operation with varying wind speed and irradiance, it is not a strict requirement for  $C_B$ ,  $C_C$ , and  $\theta_C$  to remain absolutely stable or fixed. Instead, they can fluctuate around a mean or average value as long as no significant trend or change over time is observed. Thus, it is crucial that each measurement step is sustained for several minutes to allow for the determination of mean values, as was done in the present work. More details  
130 and the step-by-step field methodology are described in section 2.3.

## 2.2. Study site and campaign

The selected study site (54.9396°S; 67.6419°W) is a 46,000 m<sup>2</sup> peatland, locally called “Omora peatland” in reference to the Omora Ethnobotanical Park (Rozzi et al., 2006) where it is located, at 2 km west of Puerto Williams, on the northern coast of  
135 Navarino Island. This peatland has been also previously called “Caleta Robalo” in a detailed study of the late quaternary vegetation and climate (Heusser et al., 1989). In that study, the age of the peatland has been established to a maximum of 13,000 y B.P. This ombrotrophic elevated peatland is dominated by *Sphagnum magellanicum*, with a hummocky topography covered by irregular patches of *Empetrum rubrum*, *Gaultheria* spp., *Marsippospermum grandiflorum*, *Tetroncium magellanicum*, *Polytrichum* spp. and shrubby Antarctic beech (*Nothofagus antarctica*). Also, several lichen species common  
140 to the Magellanic moorland complex were extensively covering the peatland, such as *Pseudocyphelaria* spp., *Cladonia* spp. and *Ochrolechia* spp. In some locations, apparent black peat was observed without a living *Sphagnum* cover. The depth of the peat layer was measured from 3 to 10 m, and the section where measurements were made was characterized by a depth of  $8 \pm 1$  m. The peatland was not flooded but the water table was close to the surface, *i.e.* 0.1–0.6 m. The water table depth was manually measured using a groundwater monitoring well, which consisted of a plastic 2-inch perforated tubing installed two  
145 days before our measurements, in close vicinity to our measurement site. The height of each measurement point, relative to the water table, was determined using a water level hose. The campaign took place on March 3–24, 2022, which corresponds to the end of summer season and to a month with relatively warm temperatures and high precipitation levels (Figure S2). To minimize the impact of operators on the peatland superficial structure, operators were using snowshoes and each measurement spot was marked prior to measurements, with a plastic ring of the same size than the chamber, to avoid stepping over the  
150 location.

## 2.3. Chamber design and fluxes measurements

The chamber was a pyramidal trunk basket with a base (opening) of  $0.32 \times 0.29$  m, and a height of 0.22 m (Model 47970, Spectrum, Mexico). Above the chamber, we positioned a low-density polyethylene film ( $1.4 \times 1.4$  m; 0.025 mm thick; Frost King, Mexico). The plastic film was adjusted and fixed to the chamber’s bottom (Fig. S1). The chamber was equipped with a  
155 battery-operated fan (Portable Fan, Cazokasi, Mexico), which was fixed on a lateral face of the chamber (opposite side from

the sun) and operated at an airflow speed of about  $1.2 \text{ m s}^{-1}$ . Inside the chamber, a light/temperature data logger was installed at ground level (MX2202, Hobo, USA), and a second one was installed on the top of the chamber. Data loggers recorded visible light intensity in Lux units. Inside the chamber, two 6 mm external diameter (4 mm internal diameter) flexible polyurethane tubing (PUN-6X1-DUO-BS, Festo, Mexico) were fixed on opposite faces of the basket, at about two-thirds of the chamber's height, passed from below the edge of the chamber and connected the UGGA. The UGGA measured  $\text{CH}_4$  and  $\text{CO}_2$  concentration at a 1 Hz frequency. When fluxes were measured, the chamber was placed face down, the plastic skirt was expanded around the chamber and a steel chain ( $0.27 \text{ kg m}^{-1}$ ) was placed above the plastic film, surrounding three times the base of the chamber to ensure that the plastic film was in contact with the ground. At the end of each experiment, a dark screen was placed above the chamber, to measure  $\text{CO}_2$  flux in absence of light (respiration from soil and plants).

Each flux measurement involved a four steps protocol (Table 1).

Step 1, the ground air concentration ( $C_L$ ) of  $\text{CH}_4$  ( $C_{L,\text{CH}_4}$ ) and  $\text{CO}_2$  ( $C_{L,\text{CO}_2}$ ) was measured for 5 min, just above the vegetation cover (where the chamber was placed).

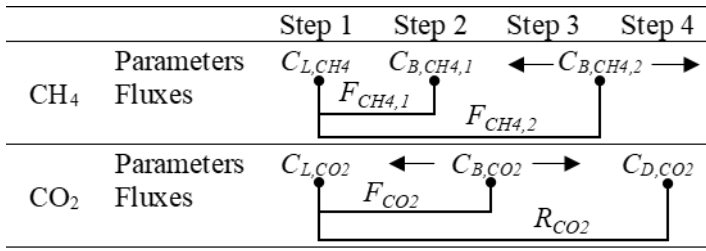
Step 2, the chamber was positioned on the ground and, once steady state was reached,  $C_B$  of  $\text{CH}_4$  ( $C_{B,\text{CH}_4}$ ) and  $\text{CO}_2$  ( $C_{B,\text{CO}_2}$ ) were measured over a 5 minutes period. It should be noted that, after pulse injection (third step), a second  $C_{B,\text{CH}_4}$  was determined. Thus  $C_{B,\text{CH}_4}$  determined during this step 2, was renamed  $C_{B,\text{CH}_4,1}$ .

Step 3, a pulse of 1 mL of standard  $\text{CH}_4$  (99.99%, Linde, Chile) was injected once with a plastic syringe through a septum connected on the waste line of the UGGA (returning to the chamber). It is worth noting that, to avoid the use of a heavy gas cylinder, the  $\text{CH}_4$  used for pulses was contained in small 0.12 L serological bottle, which were used several times before being replaced. The decreasing section of  $\text{CH}_4$  concentration was used to calibrate Equation 8, and to determine  $\theta_C$  and  $C_{B,\text{CH}_4}$ , the latter being in this case  $C_{B,\text{CH}_4,2}$ . This step was maintained for 5 to 7 minutes, until a stable  $C_{B,\text{CH}_4,2}$  was observed. It should be also noted that, as we will show in the results section, the pulse injection (*i.e.*, step 3) had no effect on the  $\text{CO}_2$  concentration within the chamber. Thus,  $C_{B,\text{CO}_2}$  could be determined over the entire period of steps 2 and 3.

Step 4, a dark screen was placed on the chamber for 5 minutes to measure  $\text{CO}_2$  flux in absence of light (respiration). This new  $\text{CO}_2$  steady state concentration was called  $C_{D,\text{CO}_2}$ ; where D stands for dark conditions. As we will show in the results section, the dark screen had no apparent effect on the  $\text{CH}_4$  concentration within the chamber. Therefore,  $C_{B,\text{CH}_4,2}$  could be determined throughout steps 3 and 4 (Table 1).

The four steps experimental strategy allowed to determine three key  $\text{CH}_4$  concentrations ( $C_{L,\text{CH}_4}$ ,  $C_{B,\text{CH}_4,1}$ , and  $C_{B,\text{CH}_4,2}$ ) that were used to determine two equivalent  $\text{CH}_4$  fluxes ( $F_{\text{CH}_4,1}$  and  $F_{\text{CH}_4,2}$ ; Eq. 5, Table 1). Similarly, three key  $\text{CO}_2$  concentrations ( $C_{L,\text{CO}_2}$ ,  $C_{B,\text{CO}_2}$ , and  $C_{D,\text{CO}_2}$ ) were determined, providing one  $\text{CO}_2$  flux and one respiration rate ( $F_{\text{CO}_2}$  and  $R_{\text{CO}_2}$ , respectively) using Equation 5 in both cases.

**Table 1:** Experimental strategy, parameters and fluxes determined (see text for details).



190 At the end of each measurement, before removing the chamber, plastic rulers were placed around the base of the chamber to mark the covered area. A photograph was taken and used to identify the extent of the area covered by the major plant species where fluxes were measured. These scaled photographs were analyzed using the Fiji software (Schindelin et al., 2012). The cover percentage of each individual species or group of species was determined using the freehand selection tool.

#### 195 2.4. Calibration and laboratory experiments

The chamber volume was experimentally checked in the laboratory (no wind) and on a flat surface, which minimizes leakage. Pulses of known volumes of CH<sub>4</sub> were injected and the concentration in the chamber was measured. The concentration curve was well modeled using the Levenspiel's equation (Levenspiel, 1999) for two continuous stirred tank reactors in series (Eq. 9).

$$200 \quad C_t = C_p \cdot \left(\frac{t}{\theta}\right) \cdot e^{\left(\frac{-t}{\theta}\right)} = \frac{M_p}{V_C} \cdot \left(\frac{t}{\theta}\right) \cdot e^{\left(\frac{-t}{\theta}\right)} \quad (9)$$

Where  $C_t$  is the concentration at time  $t$ , and  $C_p$  is the initial pulse concentration within the chamber, which is equal to the mass of CH<sub>4</sub> injected during the pulse ( $M_p$ ) divided by  $V_C$ . In Equation 9,  $C_p$  and  $\theta$  were the adjustment parameters calibrated numerically (Section 2.5).

205 In each experiment, both in the laboratory and field, the area covered by the skirt-chamber was determined from a scaled photograph of the chamber taken from above and assuming that the perimeter of the chain used to maintain the skirt in contact to the ground defined the area. The scaled photographs were treated using ImageJ (v. 1.8.0\_172).

The skirt-chamber method was validated in the field, *i.e.* on uneven terrain and exposed to wind. With that purpose, triplicate/quadruplicate pulses of six known CH<sub>4</sub> mass ( $M_p$ ) were injected into the chamber. The mass of CH<sub>4</sub> detected, in excess to the baseline, was determined through integration (Eq. 10) and compared to the mass injected. An equivalency 210 between the mass of CH<sub>4</sub> injected and the mass of it that is detected would indicate that the mass balance of the chamber is correct and that any amount of gas reaching the chamber is correctly appraised.

$$M_p = \int_0^t (C_{c,t} - C_B) \cdot \left(\frac{V_C}{\theta_C}\right) \cdot dt \quad (10)$$

## 2.5. Data treatment and statistical analysis

Equations 8, 9, and 10 were calibrated to experimental data using a Generalized Reduced Gradient (GRG) Nonlinear tool and minimizing the root mean square error (RMSE) between experimental data and models. To estimate uncertainties of flux determinations (based on Eq. 5), we considered the uncertainties linked to the measurements of the gas concentration at ground level ( $\sigma_{C_L}$ ) and of the baseline concentration ( $\sigma_{C_B}$ ) using a propagation of error approach (Eq. 11), where  $\sigma_F$  is the standard deviation of the flux determination.

$$\sigma_F = \frac{\sigma_{(C_L - C_B)}}{\theta_C} \cdot \frac{V_C}{A_C} = \frac{\sqrt{\sigma_{C_L}^2 + \sigma_{C_B}^2}}{\theta_C} \cdot \frac{V_C}{A_C} \quad (11)$$

In order to estimate the temporal and spatial variability of flux measurements on different days and locations, we used the mean coefficient of variation (CV), which is defined as the ratio of the standard deviation to the mean. When comparing fluxes measured with different methods and their corresponding CV, data were  $\text{Log}_{10}$  transformed to fulfil the normality condition assessed by Saphiro Wilk test. Then, we determined significant differences among variables using independent samples t-Test to with a  $p < 0.05$ . Model calibrations and statistical analyses were performed with Origin(Pro) OriginLab Corporation (Version 2016, Northampton, USA). Regarding the limit of detection (LOD) of the skirt-chamber method, we used the typical arbitrary limit of a minimal signal at least three times above standard deviation, thus corresponding to a CV below 33%. Measurements obtained with a higher CV were considered uncertain.

## 3. Results and discussion

### 3.1. Performance of the skirt-chamber

An example of chamber deployment in the field and the corresponding data obtained at a location where high emission was observed is shown on Figure 2. During step 1, before chamber deployment, the  $\text{CH}_4$  and  $\text{CO}_2$  concentrations at ground level, *i.e.*  $C_{L,CH_4}$  and  $C_{L,CO_2}$ , respectively, were registered. Immediately after chamber deployment (step 2), an increase of  $\text{CH}_4$  concentration was standardly observed, at a new level  $C_{B,CH_4,1}$ , which is an indicator of  $\text{CH}_4$  emissions. On the contrary, the  $\text{CO}_2$  concentration decreased to a level  $C_{B,CO_2}$ , often below  $C_{L,CO_2}$ , which is an indication of  $\text{CO}_2$  capture. On step 3, as expected, the injection of a  $\text{CH}_4$  pulse caused a sudden increase of  $\text{CH}_4$  concentration, followed by an asymptotic and slow return to the baseline level  $C_{B,CH_4,2}$ . Then, the use of a dark screen (step 4), caused an increase of the  $\text{CO}_2$  concentration at  $C_{D,CO_2}$ , above  $C_{L,CO_2}$ , which is a manifestation of respiration without photosynthetic uptake. Notably, it was observed that the  $\text{CH}_4$  pulse injection during step 3 had no effect on the  $\text{CO}_2$  concentration, and conversely, the dark screen installed during step 4 had no effect on  $\text{CH}_4$  concentration, in such manner that to improve the quality of our data,  $C_{B,CH_4,2}$  was determined using data from steps 3 and 4, while  $C_{B,CO_2}$  was determined with data from steps 2 and 3 (Table 1).



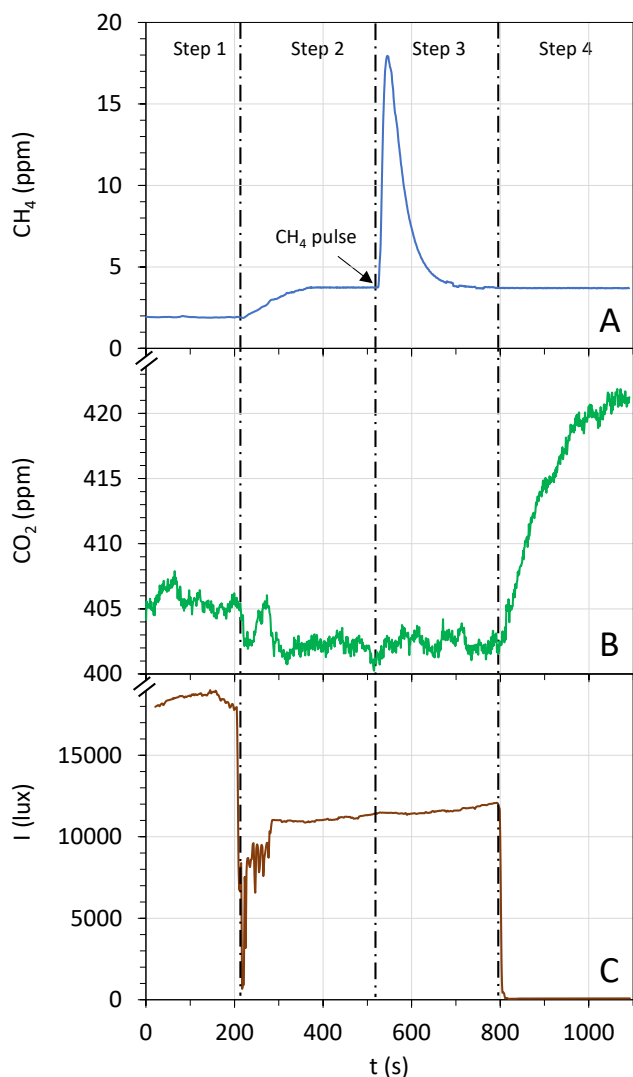


**Figure 2. Example of data obtained during a chamber deployment; (A) CH<sub>4</sub> concentration, (B) CO<sub>2</sub> concentration, and (C) visible light irradiance. See text for a complete description of the four steps.**

### 245 3.2. Calibration and method validation

In general, after pulse injections, Equation 8 fitted well the experimental data and over 130 measurements, the mean coefficient of determination ( $R^2$ ) value between the model and the experimental data was  $0.987 \pm 0.055$ , (mean  $\pm \sigma$ ), suggesting that the skirt-chamber acted as a continuously stirred tank reactor. Overall,  $\theta_C$  was estimated at  $30.74 \pm 22.70$  s during the entire field campaign. Reminding that  $\theta_C = V_C/Q_L$ , the equivalent gas flow rate exchange between the chamber and the environment (leak  
 250 flowrate) was  $0.67 \pm 0.49$  L s<sup>-1</sup>. The variations in  $\theta_C$  observed over the entire field campaign were likely influenced by weather

conditions, particularly wind variations, as well as the variable ground surface with different plant covers and, consequently, different permeabilities (see Table S2). By comparison, during laboratory testing, over a flat surface and under no wind conditions,  $\theta_C$  was estimated to  $327.13 \pm 11.24$  s ( $n = 5$ ), which corresponded to an exchange flowrate of  $0.063 \pm 0.002$  L s<sup>-1</sup>, *i.e.* ten time lower than in the field. These results suggest that the design of the skirt-chamber, simply placed on top of the vegetation rug and under non-flooded conditions, promoted a large air exchange with the environment, probably due to wind flushing the interwoven stems, leaves, and roots, at the surface of the peatland and beneath the plastic skirt. This has been the subject of a report from Lai et al. (2012) who stressed-out the importance of wind effects and might be a potential advantage of the skirt-chamber compared to standard chambers using collars, where wind effects are impeded.

During field deployment, a set of validation experiments was performed through the injection of triplicate/quadruplicate CH<sub>4</sub> samples at six distinct concentrations. In each case,  $C_{B,CH_4,2}$  and  $\theta_C$  were estimated through Eq. 8 and then the mass of CH<sub>4</sub> detected in the skirt-chamber ( $M_p$ ) was estimated using Eq. 10. The results obtained are presented in Figure 3, showing that R<sup>2</sup> was 0.997 and the slope of the mass of CH<sub>4</sub> detected vs. the mass injected was 0.977. The equivalency between the mass of CH<sub>4</sub> injected and detected indicates, first, that the mass of CH<sub>4</sub> injected was recovered without being lost due to diffusion into the ground. Indeed, it is essential to note that the transitory and artificial increase of  $C_C$  after pulse injection, has the potential to modify the concentration gradient between the chamber and the soil, as previously suggested (Kutzbach et al., 2007; Juszczak, 2013), and to promote CH<sub>4</sub> diffusion from the chamber to the soil, leading to potential biases in  $\theta_C$  determination. The consistency between the mass of CH<sub>4</sub> injected and detected also suggests that the mass balance of the skirt-chamber (Eq. 3) correctly describes the behavior of the skirt-chamber and that any amount of gas reaching the chamber is correctly accounted for, validating the method.

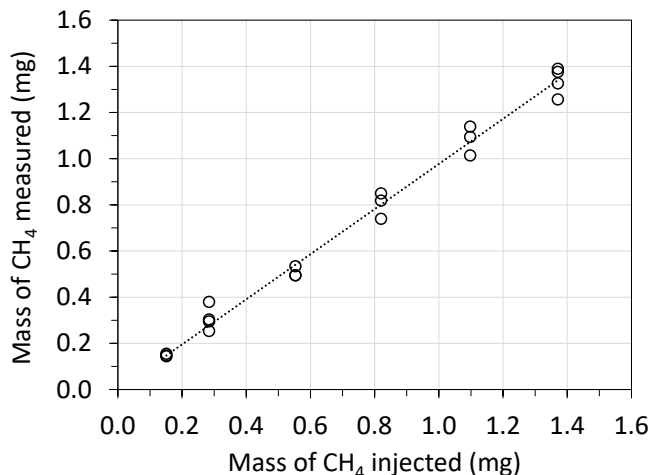


**Figure 3. Validation of the skirt-chamber through the injection of CH<sub>4</sub> pulses at different concentrations, and determination of mass of CH<sub>4</sub> detected in the chamber. Replicates measurements indicated a mean CV of  $7.1 \pm 5.0\%$ .**

### 3.3. CH<sub>4</sub> emission

275 As previously mentioned, Equation 5 used to determine CH<sub>4</sub> flux can be applied from  $C_{L,CH_4}$  and  $C_{B,CH_4,1}$  to determine  $F_{CH_4,1}$  or alternatively  $C_{L,CH_4}$  and  $C_{B,CH_4,2}$  to determine  $F_{CH_4,2}$ . We observed that  $F_{CH_4,1}$  was subject to large variations, with a mean CV of  $171 \pm 370\%$ , over 130 measurements. Contrastingly,  $F_{CH_4,2}$  was characterized by a mean CV of  $30 \pm 38\%$ . We hypothesize that the large difference in CV between  $F_{CH_4,1}$  and  $F_{CH_4,2}$  was due to two factors. First,  $C_{B,CH_4,1}$  was determined during step 2, shortly after positioning the chamber, while  $C_{B,CH_4,2}$  was determined during step 3, at least 5 minutes after the chamber was installed. Second,  $C_{B,CH_4,1}$  was determined from a shorter period of time (3 to 4 minutes) while  $C_{B,CH_4,2}$  was determined from a longer period, i.e. periods 3 and 4, lasting 8 to 9 minutes. From these results, only  $F_{CH_4,2}$  was considered hereafter.

To evaluate the repeatability of our measurements, five measurements of  $F_{CH_4,2}$  were done over a short period of time ( $< 1.5$  h) in two locations where relatively high and low emissions were observed. At the relatively high emission hotspots,  $F_{CH_4,2}$  was  $17.10 \pm 1.77$  mg m<sup>-2</sup> h<sup>-1</sup> (CV 10.3%) while at the relatively low emission spot,  $F_{CH_4,2}$  was  $1.20 \pm 0.89$  mg m<sup>-2</sup> h<sup>-1</sup> (CV 74.6%). Repeatability within a longer time frame was also evaluated with measurements at 16 locations divided in four transects of 3 m, thus separated by about 1 m. These measurements were repeated on three occasions, i.e. 2 and 12 days after the first measurement (Table 2). During these measurements, we observed that the temporal variation (same locations at different days) was characterized by a mean CV of  $59 \pm 21\%$  while the mean CV of spatial variation (different locations on the same day) was  $220 \pm 34\%$ . In particular, it was observed that the CH<sub>4</sub> hotspots, i.e. the three locations among the 16 measured where the higher fluxes were observed, did not change over time. These results suggest that the spatial variation was higher than temporal variation and that the skirt-chamber successfully detected hotspots in repeated occasions.

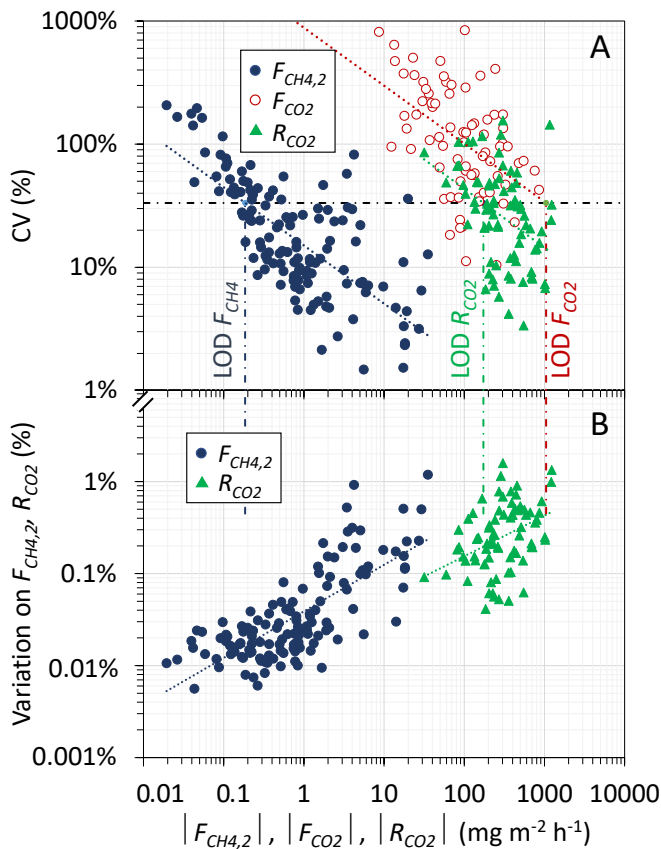
**Table 2:**  $F_{CH_4,2}$  (mg m<sup>-2</sup> h<sup>-1</sup>) measured at 16 locations divided in four transects, on three occasions, i.e. at  $t = 0, 2,$  and 12 days.

295 \*: hotspots.

#	Transect	t (d)			CV
		0	2	12	
1	1	$0.239 \pm 0.127$	$0.06 \pm 0.034$	$0.368 \pm 0.049$	70%
2	1	$0.191 \pm 0.037$	$0.078 \pm 0.083$	$0.224 \pm 0.065$	47%
3	1	$1.069 \pm 0.047$	$0.053 \pm 0.07$	$0.744 \pm 0.058$	83%
4	1	$0.564 \pm 0.108$	$0.005 \pm 0.042$	$0.326 \pm 0.031$	94%
5	2	$1.911 \pm 0.14$	$0.687 \pm 0.114$	$0.808 \pm 0.117$	59%
6	2	$8.026 \pm 0.529^*$	$5.338 \pm 0.99^*$	$4.446 \pm 0.719^*$	31%
7	2	$0.307 \pm 0.091$	$1.477 \pm 0.077$	$0.676 \pm 0.148$	73%
8	2	$3.880 \pm 0.233$	$0.938 \pm 0.133$	$3.15 \pm 0.299$	58%
9	3	$30.600 \pm 1.840^*$	$44.980 \pm 2.454^*$	$19.215 \pm 0.845^*$	41%

10	3	$1.07 \pm 0.093$	$1.907 \pm 0.110$	$0.120 \pm 0.062$	87%
11	3	$6.708 \pm 0.283^*$	$5.097 \pm 0.817^*$	$5.912 \pm 0.370^*$	14%
12	3	$1.753 \pm 0.032$	$2.806 \pm 0.232$	$1.254 \pm 0.112$	41%
13	4	$1.284 \pm 0.135$	$1.997 \pm 0.07$	$0.417 \pm 0.045$	64%
14	4	$0.134 \pm 0.04$	$0.170 \pm 0.057$	$0.351 \pm 0.04$	53%
15	4	$1.570 \pm 0.087$	$2.060 \pm 0.09$	$0.323 \pm 0.053$	68%
16	4	$0.485 \pm 0.136$	$0.311 \pm 0.119$	$0.107 \pm 0.082$	63%
Mean		$3.737 \pm 7.533$	$4.248 \pm 10.992$	$2.403 \pm 4.799$	28%
CV		202%	259%	200%	

The error on  $F_{CH_4,2}$  determination was evaluated through CV (Eq. 11; Fig. 4A). As flux is determined from the difference of  $C_L$  and  $C_B$ , the smaller is that difference, the smaller is the flux and the larger is the impact of measurement noise. Overall, CV ranged from 1 to 207% with a mean of  $30 \pm 38\%$ , with obvious larger CV for lower fluxes. It is worth noting that large errors on low flux measurements would have a relatively little impact on the mean emission that would be attributed to a peatland, particularly if it includes hotspots. For instance, in the set of 16 measurements (Table 2), the three locations with the larger emissions represented 76-82% of the total emission. Thus, the remaining 18-24% of the emissions were distributed among 13 relatively low emission spots, for which a measurement error has a little specific weight. To illustrate the latter, based on our complete dataset (130 measurements), we determined how the variation in each measurement, propagates to the mean emission of the complete dataset ( $\bar{F}_{CH_4,2}$ ; Figure 4B). Clearly, although hotspots are characterized by a lower CV, they have a much larger impact on the mean emission, compared to low emission spots. Hotspots must therefore be the object of a closer attention, when determining the mean emission of a peatland. As it will be discussed in section 3.6, this is a potential strength of the skirt-chamber, because it allows to multiply the number of locations that can be characterized in a given timeframe, offering a higher probability to detect hotspots.



310

**Figure 4. Impact of the absolute magnitude of flux and respiration on the coefficient of variation (CV), and limit of detection of the method (LOD; A); impact of each  $F_{CH_4,2}$  measurement of the mean emission of the complete dataset (B).**

Regarding the LOD of the  $CH_4$  flux determination, we used the typical arbitrary limit of a CV below 33%. This was the case of 71 % of our complete set of  $F_{CH_4,2}$  measurements. When applying the CV limit to the power trendline that best fitted our  
 315 experimental data ( $CV = 0.15 \cdot F_{CH_4,2}^{-0.472}$ ; Fig. 4A), we estimated that the LOD of  $|F_{CH_4,2}|$  was  $0.185 \text{ mg m}^{-2} \text{ h}^{-1}$ , and 81% of our complete dataset ( $n=130$ ) was above that LOD. If considering all measurements inferior to LOD uncertain and equal to zero, the mean emission of the whole dataset was reduced by only 0.7%. Thus, as previously established, measurements with low significance had a negligible impact on the mean emission.

Overall, the  $CH_4$  flux ranged between  $-4.23$  and  $35.26 \text{ mg m}^{-2} \text{ h}^{-1}$ , with a mean magnitude of  $2.68 \pm 6.05 \text{ mg m}^{-2} \text{ h}^{-1}$ . This range  
 320 is consistent with values reported in previous measurements conducted in peatlands from Southern Patagonia, which were ranging between  $-0.03$  and  $17.30 \text{ mg m}^{-2} \text{ h}^{-1}$  (Münchberger et al., 2019; Barret et al., 2022). Approximately 80% of  $CH_4$  fluxes were below those reported by Münchberger et al. (2019), Lehmann et al. (2016), and Fritz et al. (2011) using the static chamber method. Our  $CH_4$  fluxes are also in the same order of magnitude of fluxes reported from bogs and fens in northern regions  
 325 the largest reported in tropical peatlands (Ribeiro et al., 2021); for example, in Panama ( $31$  and  $48 \text{ mg m}^{-2} \text{ h}^{-1}$ ) (Wright et al.,

2013; Hoyos-Santillan et al., 2019) and in Venezuela (40.03 mg m<sup>-2</sup> h<sup>-1</sup>) (Bracho et al., 1990). Negative values were observed in 11% of measurements, most of them being close to the detection limit of the method. When excluding negative values, the range of CH<sub>4</sub> emissions covered three orders of magnitude, sometimes on very close locations.

### 3.4. CO<sub>2</sub> emissions

330 Overall, CO<sub>2</sub> readings were subject to a higher noise level, compared to CH<sub>4</sub> readings, and therefore  $F_{CO_2}$  presented higher variability. Overall,  $F_{CO_2}$  was negative in 54% of the cases, and ranged between -857 and 549 mg m<sup>-2</sup> h<sup>-1</sup>, with a mean of -21.56 ± 208.49 mg m<sup>-2</sup> h<sup>-1</sup>. This large variability was reflected in the CV of the absolute  $F_{CO_2}$ , noted  $|F_{CO_2}|$  (Fig. 4A), which were significantly higher than the corresponding CV of  $F_{CH_4}$  ( $p < 0.05$ ). In this case, the LOD of  $|F_{CO_2}|$  was estimated to 1,047 mg m<sup>-2</sup> h<sup>-1</sup> and none of our measurements was above that limit. Moreover, only 10% of our measurements presented a  
 335 CV inferior to 33.3%. These results provide strong evidence that the skirt-chamber, in its present configuration, inaccurately estimated the CO<sub>2</sub> exchange between the peatland and the atmosphere, primarily due to the highly fluctuating CO<sub>2</sub> concentrations combined with relatively low CO<sub>2</sub> emission/capture rates. Indeed, in contrast to  $C_{B,CH_4}$ ,  $C_{B,CO_2}$  exhibited high dependence on solar irradiance, which was rapidly changing during the field campaign. Therefore, our first suggestion would be to deploy the chamber under more stable irradiance conditions possible. Furthermore, the skirt-chamber tested utilized a  
 340 transparent plastic film over a basket made of sparsely interwoven steel wires, resulting in limited light penetration to the ground, estimated at 54 ± 8%. Hence, our second suggestion would be to optimize incoming irradiance to better mimic the actual conditions existing in the field. This could be achieved through a more transparent chamber design, ensuring that the photosynthetic activity within the chamber closely approximates the conditions that the plants would experience under natural conditions, without a chamber.

### 345 3.5. Ecosystem respiration

As illustrated on Figure 2, when covering the skirt-chamber with a dark screen, i.e. when photosynthetic activity was inhibited, an increase of the CO<sub>2</sub> concentration within the skirt-chamber was standardly observed, reaching a new steady state at  $C_{D,CO_2}$ , corresponding to the ecosystem respiration. This behavior was observed in all cases and suggested that the respiration rate can be measured during field deployment of the skirt-chamber. The dark screen limited light penetration by 98.4 ± 1.8%, in such  
 350 manner that photosynthesis could be considered insignificant. The change of the CO<sub>2</sub> concentration, from  $C_{B,CO_2}$  to  $C_{D,CO_2}$ , was relatively fast and followed an asymptotic trend similar to Eq. 8 (Eq. 12), where  $C_{C,CO_2,t}$  is the CO<sub>2</sub> chamber concentration at time  $t$ , and  $\theta_D$  is the response time.

$$C_{C,CO_2,t} = C_{D,CO_2} + (C_{B,CO_2} - C_{D,CO_2}) \cdot e^{\left(-\frac{t}{\theta_D}\right)} \quad (12)$$

Equation 12 described well the experimental data, with a mean R<sup>2</sup> of 0.879 ± 0.156. Overall,  $\theta_D$  was 53.7 ± 31.3 s, which  
 355 indicates a fast metabolic change after the switch from light to dark conditions, in accordance with the literature (Masarovičová, 1979). Overall,  $R_{CO_2}$  was positive, i.e. CO<sub>2</sub> emission, in all but two cases, with a range (excluding negative values) of 31–1231

mg m<sup>-2</sup> h<sup>-1</sup> and a mean of 359 ± 292 mg m<sup>-2</sup> h<sup>-1</sup>. This range is consistent with those previous reports conducted in peatlands from Southern Patagonia, which ranged between 8 and 667 mg m<sup>-2</sup> h<sup>-1</sup> using the traditional static chamber method (Pancotto et al., 2021; Barret et al., 2022). Regarding repeatability,  $R_{CO_2}$  was also evaluated with measurements at 16 locations divided  
360 in four transects of 3 m, on three occasions, *i.e.* 2 and 12 days after the first measurement (Table S1). During these measurements, we observed that the temporal variation (same location at different days) was characterized by a mean CV of 33 ± 17% while the mean CV of spatial variation (different locations on the same day) was 58 ± 5%. These values suggest two important patterns. First, that  $R_{CO_2}$  is relatively well distributed, as compared to  $F_{CH_4,2}$ . Second, that the temporal variation of  $R_{CO_2}$  is lower than its spatial variation; this pattern resembles the findings for  $F_{CH_4,2}$ .  
365 The CV of the absolute  $R_{CO_2}$ , noted  $|R_{CO_2}|$  (Fig. 4A), was within the same range than the CV of  $F_{CH_4,2}$ . In this case the LOD of  $|R_{CO_2}|$  was estimated to 173 mg m<sup>-2</sup> h<sup>-1</sup> and 76% of our measurements were above that limit. As previously done with  $F_{CH_4,2}$ , we also determined how the variation in each measurement propagates to the mean respiration of the complete dataset (Figure 4B). Although with a larger impact than in the case of  $F_{CH_4,2}$ , similar results were obtained. These results suggest that the skirt-chamber allowed the accurate determination of the ecosystem respiration. In this case too, no correlation was found  
370 between  $R_{CO_2}$  (Table S1) and the coverage of plants (Table S2).

### 3.6. Strengths, weaknesses and perspectives of the skirt-chamber

The skirt-chamber concept, tested for the first time in this work, allowed for the determination of CH<sub>4</sub> emissions and respiration rates in a peatland. For both parameters, the majority of the measurements were above the detection limit of the method and were characterized by a CV within acceptable limits (*i.e.* <33%). By repeating measurements over a 12-days period, similar  
375 results were obtained, indicating that these parameters were more homogeneously distributed over time than over space. From the experience acquired during field deployment, the best strategy would be to measure CH<sub>4</sub> emissions and ecosystem respiration according to a three-steps protocol: (i) measurement of ground-air concentration for 5 min, followed by (ii) the installation of the chamber and the immediate pulse injection, waiting 5-7 minutes before (iii) covering the chamber with a dark screen for an additional 5 min. Thus, in 15-17 min, CH<sub>4</sub> emission and ecosystem respiration of a specific location can be  
380 determined, which suggest that about 20–30 locations could be measured in a reasonable workday (even in remote areas). The main strength of the method is that these parameters can be determined in a minimally intrusive manner and without delay. Moreover, the relatively small size of the skirt-chamber also allows to determine CH<sub>4</sub> emission and respiration with a good spatial resolution, on almost any terrain and vegetation cover. However, several points still require a close attention that we discuss as follows:

385 First, the mass balance of the skirt-chamber (Section 2.1) is sensitive to varying wind speed and solar irradiance, affecting  $\theta_C$ ,  $C_B$  and  $C_C$ . To this regard, it should be noted that it is not a strict requirement for  $C_B$ ,  $C_C$ , and  $\theta_C$  to remain absolutely stable or fixed, as long as these parameters fluctuate around a mean value with no significant trend or change over time, and that each measurement step is sustained for several minutes. During our experiments, we conducted quadruplicate measurements of

known CH<sub>4</sub> samples at six distinct concentrations (Figure 3), and the results indicated a mean CV of  $7.1 \pm 5.0\%$ . This suggests  
390 that external conditions, not related to ecosystem emission variability, had a relatively limited impact on measurements. The  
validity of this finding was further confirmed through quintuplicate ecosystem flux measurements ( $F_{CH_4,2}$ ), which showed a  
CV of 10.3% at a relatively high emission hotspot and a CV of 74.6% at a relatively low emission spot. This indicates that the  
variation in parameters estimation was primarily due to fluctuations of ecosystem emissions, rather than changing  
environmental conditions. However, we acknowledge that varying environmental conditions might still have some impact,  
395 and we hypothesize that using a wind shield in close vicinity to the chamber might reduce the influence of wind gusts and to  
improve the accuracy of the method, which should be tested.

Second, during chamber deployment, we typically observed moderate temperature increases, as exemplified in Figure S3,  
ranging from 0 to 4.25 °C with a mean of  $0.83 \pm 1.30$  °C above the ambient air temperature, over the chamber deployment  
time. The slope of the temperature increase ranged from 0 to 0.63 °C min<sup>-1</sup>, with a mean of  $0.09 \pm 0.15$  °C min<sup>-1</sup>. This  
400 temperature increase was positively correlated with sun irradiance, with a Pearson correlation factor of  $r(130) = 0.712$  ( $p <$   
 $0.05$ ). The correlation between the temperature change rate ( $dT dt^{-1}$ ) and sun irradiance ( $I$ ) was described by the equation  $dT/dt$   
 $= -0.178 + 2.54 \times 10^{-5} I$ . In some cases, a decrease in temperature was observed, associated with a sudden decrease in sun  
irradiance, and this cooling effect was systematically observed after the dark screen was placed on the chamber for respiration  
measurement (step 4). We attribute the relatively moderate temperature increases to two main factors. First, as a characteristic  
405 of the skirt-chamber, there is a constant gas exchange with the exterior, thus reducing heat accumulation within the chamber  
that would be observed in a closed chamber. Second, the light intensity was moderated due to the relatively low latitude of the  
Navarino Island (54.9396°S) and the lack of transparency of the chamber (as discussed in Section 3.4).

Third, in this study, we exclusively tested the chamber under non-flooded conditions. However, it is expected that the chamber  
would function effectively when used in flooded areas, where a water layer would provide a seal between the chamber and the  
ground. In such cases, the chamber would likely operate similarly to a standard closed chamber without any leakage, which  
410 could be confirmed through pulse injection. However, the latter should be experimentally tested.

Fourth, another feature of the skirt-chamber is that it does not allow for the segregation of diffusive and ebullitive fluxes, well-  
documented in the literature (Baird et al., 2009). During our measurements, we did not observe sudden peak increases in CH<sub>4</sub>  
or CO<sub>2</sub> concentrations, which would be expected if bubbles were reaching the surface. Rather than dismissing ebullition, we  
415 hypothesize that this absence of peak concentrations was due to the measurements being conducted under non-flooded  
conditions. In such conditions, any bubbles reaching the acrotelm of the peatland would probably diffuse at a moderate rate  
through the organic material layer instead of being suddenly released to the gas phase. In this study, emissions were measured  
based on mean CH<sub>4</sub>/CO<sub>2</sub> concentrations during steady states, which encompassed some variations potentially associated with  
ebullition or other temporal effects. Therefore, the results obtained with the skirt-chamber reflect total emissions, and an  
420 alternative strategy should be employed to separate ebullitive fluxes.

Fifth, in the literature, it is well documented that measuring dark respiration immediately after a period of illumination might  
lead to an overestimation of plant respiration due to the process of light-enhanced dark respiration (LED<sub>R</sub>) in living plant



tissues (Atkin et al., 2000; Barbour et al., 2007; Werner et al., 2011). In our study, we adhered to a standard protocol for measuring dark respiration in peatland ecosystems, aligning our analysis with the methodology commonly employed in similar studies (Shaver et al., 2007; Järveoja et al., 2018, 2020; Capooci and Vargas, 2022; Rankin et al., 2022; Virkkala et al., 2022; Ilyasov et al., 2023). By limiting the dark periods to just 5 minutes, we aimed to reduce the potential influence of LEDR, a phenomenon that typically peaks between 10 to 20 minutes (Barbour et al., 2007; Atkin et al., 2000) and is strongly influenced by light levels, without displaying a clear pattern (Barbour et al., 2007). Nevertheless, we recognize that the possibility of LEDR affecting our respiration estimates exists in our experimental approach, and as such, the results presented in this study should be considered with appropriate caveats. Despite these considerations, we believe that our discrete gas flux measurements effectively capture the spatial variability of peatland emissions across the microtopography, an issue of significant importance in these ecosystems as discussed by Capooci and Vargas (2022).

Compared to standard chambers, i.e. non-steady-state chambers (closed systems) that are inserted/embedded into the ground with a collar, the skirt-chamber offers several key advantages. These include minimal soil disturbance, a smaller chamber size, and the absence of a collar, which allow rapid measurements in multiple locations, thus enabling improved spatial resolution, as well as improved portability, making it advantageous for fieldwork in remote locations. Furthermore, the design of the skirt-chamber may help regulate the temperature increase within the chamber, thanks to constant gas exchange with the exterior that reduces heat accumulation. Contrastingly, standard chambers, and in particular automatic chambers, offer an incomparable temporal resolution, with minimal field workload. Thus, we conclude that the skirt-chamber concept is a new alternative tool, with specific advantages, that could be advantageously combined with the existing methods, to improve our understanding of greenhouse gas emissions and of the factors controlling them in peatlands.

## **Supporting Information**

One supporting information file (Word Document .docx) containing three Figures and two Tables.

## **Author Contributions**

The manuscript was written through contributions of all authors. All authors have given approval to the final version of the manuscript.

## **Acknowledgements**

This project was financially supported by the Cape Horn International Center project (ANID, CHIC-FB210018). ANID, Fondecyt Postdoc (3220809), and Millennium Science Initiative Program (ICN2021\_002). Special thanks to Rachele Ossola for her help in preparing the graphical abstract.

## References

- Abdalla, M., Hastings, A., Truu, J., Espenberg, M., Mander, Ü., and Smith, P.: Emissions of methane from northern peatlands: a review of management impacts and implications for future management options, *Ecology and Evolution*, 6, 7080–7102, <https://doi.org/10.1002/ECE3.2469>, 2016.
- 455 AR6 Climate Change 2021: The Physical Science Basis — IPCC: <https://www.ipcc.ch/report/sixth-assessment-report-working-group-i/>, last access: 7 October 2022.
- Aubinet, M., Vesala, T., and Papale, D.: Eddy Covariance: A Practical Guide to Measurement and Data Analysis, *Springer Atmospheric Sciences*, 1, 0–438, <https://doi.org/10.1007/978-94-007-2351-1>, 2012.
- Atkin, O. K., Evans, J. R., Ball, M. C., Lambers, H., and Pons, T. L.: Leaf Respiration of Snow Gum in the Light and Dark.
- 460 Interactions between Temperature and Irradiance, *Plant Physiol*, 122, 915–924, <https://doi.org/10.1104/PP.122.3.915>, 2000.
- Baird, A. J., Belyea, L. R., and Morris, P. J.: Upscaling of Peatland-Atmosphere Fluxes of Methane: Small-Scale Heterogeneity in Process Rates and the Pitfalls of “Bucket-and-Slab” Models, *Carbon Cycling in Northern Peatlands*, 37–53, <https://doi.org/10.1029/2008GM000826>, 2013.
- Barbour, M. M., McDowell, N. G., Tcherkez, G., Bickford, C. P., and Hanson, D. T.: A new measurement technique reveals
- 465 rapid post-illumination changes in the carbon isotope composition of leaf-respired CO<sub>2</sub>, *Plant Cell Environ*, 30, 469–482, <https://doi.org/10.1111/J.1365-3040.2007.01634.X>, 2007.
- Barret, M., Gandois, L., Thalasso, F., Martinez-Cruz, K., Sepulveda-Jauregui, A., Lavergne, C., Teisserenc, R., Aguilar-Muñoz, P., Gerardo-Nieto, O., Etchebehere, C., Dellagnezze, B., Bovio-Winkler, P., Fochesatto, G., Tananaev, N., Svenning, M. M., Seppey, C., Tveit, A., Chamy, R., Astorga-España, M. S., Mansilla, A. O., van de Putte, A., Sweetlove, M., and Murray,
- 470 A. E.: A combined microbial and biogeochemical dataset from high-latitude ecosystems with respect to methane cycle, *Scientific Data*, 9, 674, <https://doi.org/10.1038/s41597-022-01759-8>, 2022.
- Bracho, R. and Jose, J. J. S.: Energy Fluxes in a Morichal (Swamp Palm Community) at the Orinoco Llanos, Venezuela - Microclimate, Water-Vapor and Co<sub>2</sub> Exchange, *Photosynthetica*, 24, 468–494, 1990.
- Capooci, M. and Vargas, R.: Trace gas fluxes from tidal salt marsh soils: implications for carbon-sulfur biogeochemistry,
- 475 *Biogeosciences*, 19, 4655–4670, <https://doi.org/10.5194/BG-19-4655-2022>, 2022.
- Christiansen, J. R., Korhonen, J. F. J., Juszczak, R., Giebels, M., and Pihlatie, M.: Assessing the effects of chamber placement, manual sampling and headspace mixing on CH<sub>4</sub> fluxes in a laboratory experiment, *Plant and Soil* 2011 343:1, 343, 171–185, <https://doi.org/10.1007/S11104-010-0701-Y>, 2011.
- Cobb, A. R., Hoyt, A. M., Gandois, L., Eri, J., Dommain, R., Salim, K. A., Kai, F. M., Su’ut, N. S. H., and Harvey, C. F.: How
- 480 temporal patterns in rainfall determine the geomorphology and carbon fluxes of tropical peatlands, *Proceedings of the National Academy of Sciences*, 114, E5187–E5196, <https://doi.org/10.1073/pnas.1701090114>, 2017.

- Ding, W., Cai, Z., and Tsuruta, H.: Diel variation in methane emissions from the stands of *Carex lasiocarpa* and *Deyeuxia angustifolia* in a cool temperate freshwater marsh, *Atmospheric Environment*, 38, 181–188, <https://doi.org/10.1016/J.ATMOSENV.2003.09.066>, 2004.
- 485 Edwards, N. T. and Sollins, P.: Continuous Measurement of Carbon Dioxide Evolution From Partitioned Forest Floor Components, *Ecology*, 54, 406–412, <https://doi.org/10.2307/1934349>, 1973.
- Fritz, C., Pancotto, V. A., Elzenga, J. T. M., Visser, E. J. W., Grootjans, A. P., Pol, A., Iturraspe, R., Roelofs, J. G. M., and Smolders, A. J. P.: Zero methane emission bogs: extreme rhizosphere oxygenation by cushion plants in Patagonia, *New Phytologist*, 190, 398–408, <https://doi.org/10.1111/J.1469-8137.2010.03604.X>, 2011.
- 490 Frolking, S., Talbot, J., Jones, M. C., Treat, C. C., Kauffman, J. B., Tuittila, E. S., and Roulet, N.: Peatlands in the Earth’s 21st century climate system, <https://doi.org/10.1139/a11-014>, 19, 371–396, <https://doi.org/10.1139/A11-014>, 2011.
- Griscom, B. W., Adams, J., Ellis, P. W., Houghton, R. A., Lomax, G., Miteva, D. A., Schlesinger, W. H., Shoch, D., Siikamäki, J. v., Smith, P., Woodbury, P., Zganjar, C., Blackman, A., Campari, J., Conant, R. T., Delgado, C., Elias, P., Gopalakrishna, T., Hamsik, M. R., Herrero, M., Kiesecker, J., Landis, E., Laestadius, L., Leavitt, S. M., Minnemeyer, S., Polasky, S., Potapov, 495 P., Putz, F. E., Sanderman, J., Silvius, M., Wollenberg, E., and Fargione, J.: Natural climate solutions, *Proceedings of the National Academy of Sciences*, 114, 11645–11650, <https://doi.org/10.1073/pnas.1710465114>, 2017.
- Günther, A. B., Huth, V., Jurasinski, G., and Glatzel, S.: Scale-Dependent Temporal Variation in Determining the Methane Balance of a Temperate Fen, *Greenh Gas Meas Manag*, 4, 1, 41–48, <https://doi.org/10.1080/20430779.2013.850395>, 2014
- Günther, A., Barthelmes, A., Huth, V., Joosten, H., Jurasinski, G., Koebisch, F., and Couwenberg, J.: Prompt rewetting of 500 drained peatlands reduces climate warming despite methane emissions, *Nature Communications* 2020 11:1, 11, 1–5, <https://doi.org/10.1038/s41467-020-15499-z>, 2020.
- Heusser, C. J.: Late Quaternary Vegetation and Climate of Southern Tierra del Fuego. Late Quaternary vegetation and climate of southern Tierra del Fuego. *Quaternary Research*, 31, 3, 396–406, [https://doi.org/10.1016/0033-5894\(89\)90047-1](https://doi.org/10.1016/0033-5894(89)90047-1), 1989.
- Hoyos-Santillan, J., Lomax, B. H., Large, D., Turner, B. L., Lopez, O. R., Boom, A., Sepulveda-Jauregui, A., and Sjögersten, 505 S.: Evaluation of vegetation communities, water table, and peat composition as drivers of greenhouse gas emissions in lowland tropical peatlands, *Science of The Total Environment*, 688, 1193–1204, <https://doi.org/10.1016/J.SCITOTENV.2019.06.366>, 2019.
- Ilyasov, D. V., Meshcheryakova, A. V., Glagolev, M. V., Kupriianova, I. V., Kaverin, A. A., Sabrekov, A. F., Kulyabin, M. F., and Lapshina, E. D.: Field-Layer Vegetation and Water Table Level as a Proxy of CO<sub>2</sub> Exchange in the West Siberian 510 Boreal Bog, *Land* 2023, Vol. 12, Page 566, 12, 566, <https://doi.org/10.3390/LAND12030566>, 2023.
- Järveoja, J., Nilsson, M. B., Gažovič, M., Crill, P. M., and Peichl, M.: Partitioning of the net CO<sub>2</sub> exchange using an automated chamber system reveals plant phenology as key control of production and respiration fluxes in a boreal peatland, *Global Change Biology*, 24, 3436–3451, <https://doi.org/10.1111/GCB.14292>, 2018.
- Järveoja, J., Nilsson, M. B., Crill, P. M., and Peichl, M.: Bimodal diel pattern in peatland ecosystem respiration rebuts uniform 515 temperature response, *Nature Communications* 2020 11:1, 11, 1–9, <https://doi.org/10.1038/s41467-020-18027-1>, 2020.

- Juszczak, R.: Biases in Methane Chamber Measurements in Peatlands, *International Agrophysics*, 27, 2, 159–168, <https://doi.org/10.2478/V10247-012-0081-Z>, 2013.
- Kutzbach, L., Schneider, J., Sachs, T., Giebels, M., Nykänen, H., Shurpali, N. J., Martikainen, P. J., Alm, J., and Wilmking, M.: CO<sub>2</sub> flux determination by closed-chamber methods can be seriously biased by inappropriate application of linear regression, *Biogeosciences*, 4, 1005–1025, <https://doi.org/10.5194/BG-4-1005-2007>, 2007.
- Lai, D. Y. F., Roulet, N. T., Humphreys, E. R., Moore, T. R., and Dalva, M.: The effect of atmospheric turbulence and chamber deployment period on autochamber CO<sub>2</sub> and CH<sub>4</sub> flux measurements in an ombrotrophic peatland, *Biogeosciences*, 9, 3305–3322, <https://doi.org/10.5194/BG-9-3305-2012>, 2012.
- Lawson, I. T., Kelly, T. J., Aplin, P., Boom, A., Dargie, G., Draper, F. C. H., Hassan, P. N. Z. B. P., Hoyos-Santillan, J., Kaduk, J., Large, D., Murphy, W., Page, S. E., Roucoux, K. H., Sjögersten, S., Tansey, K., Waldram, M., Wedeux, B. M. M., and Wheeler, J.: Improving estimates of tropical peatland area, carbon storage, and greenhouse gas fluxes, *Wetlands Ecology and Management* 2014 23:3, 23, 327–346, <https://doi.org/10.1007/S11273-014-9402-2>, 2014.
- Lehmann, J. R. K., Münchberger, W., Knoth, C., Blodau, C., Nieberding, F., Prinz, T., Pancotto, V. A., and Kleinebecker, T.: High-Resolution Classification of South Patagonian Peat Bog Microforms Reveals Potential Gaps in Up-Scaled CH<sub>4</sub> Fluxes by use of Unmanned Aerial System (UAS) and CIR Imagery, *Remote Sensing* 2016, Vol. 8, Page 173, 8, 173, <https://doi.org/10.3390/RS8030173>, 2016.
- Leifeld, J. and Menichetti, L.: The underappreciated potential of peatlands in global climate change mitigation strategies, *Nature Communications* 2018 9:1, 9, 1–7, <https://doi.org/10.1038/s41467-018-03406-6>, 2018.
- Levenspiel, O.: *Chemical Reaction Engineering*, 3rd ed.; Anderson, W., Hepburn, K., Santor, K., Eds.; Times Roman by Bi-Comp Inc, 4140–4143, 1999.
- Limpert, K. E., Carnell, P. E., Trevathan-Tackett, S. M., and Macreadie, P. I.: Reducing Emissions From Degraded Floodplain Wetlands, *Frontiers in Environmental Science*, 8, 8, <https://doi.org/10.3389/FENVS.2020.00008/BIBTEX>, 2020.
- Livingston, G. and Hutchinson, J.: Enclosure-Based Measurement of Trace Gas Exchange: Applications and Sources of Error, In *Biogenic trace gases: measuring emissions from soil and water*, Matson, P., Harris, R., Eds.; R.C., Oxford, UK, 14–51, 1995.
- Masarovičova, E.: Relationships between the CO<sub>2</sub> compensation concentration, the slope of CO<sub>2</sub> curves of net photosynthetic rate and the energy of irradiance, *Biologia Plantarum* 1979 21:6, 21, 434–439, <https://doi.org/10.1007/BF02889485>, 2008.
- Münchberger, W., Knorr, K. H., Blodau, C., Pancotto, V. A., and Kleinebecker, T.: Zero to moderate methane emissions in a densely rooted, pristine Patagonian bog - Biogeochemical controls as revealed from isotopic evidence, *Biogeosciences*, 16, 541–559, <https://doi.org/10.5194/BG-16-541-2019>, 2019.
- Page, S., Mishra, S., Agus, F., Anshari, G., Dargie, G., Evers, S., Jauhiainen, J., Jaya, A., Jovani-Sancho, A. J., Laurén, A., Sjögersten, S., Suspense, I. A., Wijedasa, L. S., and Evans, C. D.: Anthropogenic impacts on lowland tropical peatland biogeochemistry, *Nature Reviews Earth & Environment* 2022 3:7, 3, 426–443, <https://doi.org/10.1038/s43017-022-00289-6>, 2022.

- 550 Pancotto, V., Holl, D., Escobar, J., Castagnani, M. F., and Kutzbach, L.: Cushion bog plant community responses to passive warming in southern Patagonia, *Biogeosciences*, 18, 4817–4839, <https://doi.org/10.5194/BG-18-4817-2021>, 2021.
- Pavelka, M., Acosta, M., Kiese, R., Altimir, N., Brümmer, C., Crill, P., Darenova, E., Fu, Gielen, B., Graf, A., Klemedtsson, L., Lohila, A., Longdoz, B., Lindroth, A., Nilsson, M., Marañón Jiménez, S., Merbold, L., Montagnani, L., Peichl, M., Pumpanen, J., Serrano Ortiz, P., Silvennoinen, H., Skiba, U., Vestin, P., Weslien, P., Janous, D., and Kutsch, W.:
- 555 Standardisation of chamber technique for CO<sub>2</sub>, N<sub>2</sub>O and CH<sub>4</sub> fluxes measurements from terrestrial ecosystems, *International Agrophysics*, 32, 569–587, <https://doi.org/10.1515/intag-2017-0045>, 2018.
- Pirk, N. and Mastepanov, M.: Calculations of automatic chamber flux measurements of methane and carbon dioxide using short time series of concentrations, *Biogeosciences* 14593–14617, <https://doi.org/10.5194/bgd-12-14593-2015>, 2015.
- Ribeiro, K., Pacheco, F. S., Ferreira, J. W., de Sousa-Neto, E. R., Hastie, A., Krieger Filho, G. C., Alvalá, P. C., Forti, M. C.,
- 560 and Ometto, J. P.: Tropical peatlands and their contribution to the global carbon cycle and climate change, *Global Change Biology*, 27, 489–505, <https://doi.org/10.1111/GCB.15408>, 2021.
- Rankin, T. E., Roulet, N. T., and Moore, T. R.: Controls on autotrophic and heterotrophic respiration in an ombrotrophic bog, *Biogeosciences*, 19, 3285–3303, <https://doi.org/10.5194/BG-19-3285-2022>, 2022.
- Rozzi, R., Armesto, J. J., Gutiérrez, J., Massardo, F., Likens, G., Anderson, C. B., Poole, A., Moses, K., Hargrove, G., Mansilla,
- 565 A., Kennedy, J.H., Willson, M., Jax, K., Jones, C., Callicott, J. B., and Kalin., M. T.: Integrating ecology and environmental ethics: Earth stewardship in the southern end of the Americas, *BioScience*, 62, 3, 226-236 <https://doi.org/10.1525/bio.2012.62.3.4>, 2012.
- Rozzi, R., Massardo, F., Anderson, C. B., Kurt Heidinger, J. A., and Silander, Jr.: Ten Principles for biocultural conservation at the southern tip of the Americas: The approach of the Omora Ethnobotanical Park, *Ecology and Society*, 11, 1, 43,
- 570 <https://www.jstor.org/stable/26267796>, 2006.
- Schindelin, J., Arganda-Carreras, I., Frise, E., Kaynig, V., Longair, M., Pietzsch, T., Preibisch, S., Rueden, C., Saalfeld, S., Schmid, B., Tinevez, J. Y., White, D. J., Hartenstein, V., Eliceiri, K., Tomancak, P., and Cardona, A.: Fiji: an open-source platform for biological-image analysis, *Nature Methods* 2012 9:7, 9, 676–682, <https://doi.org/10.1038/nmeth.2019>, 2012.
- Shaver, G. R., Street, L. E., Rastetter, E. B., Van Wijk, M. T., and Williams, M.: Functional convergence in regulation of net
- 575 CO<sub>2</sub> flux in heterogeneous tundra landscapes in Alaska and Sweden, *Journal of Ecology*, 95, 802–817, <https://doi.org/10.1111/J.1365-2745.2007.01259.X>, 2007.
- Swails, E., Hergoualc’h, K., Verchot, L., Novita, N., and Lawrence, D.: Spatio-Temporal Variability of Peat CH<sub>4</sub> and N<sub>2</sub>O Fluxes and Their Contribution to Peat GHG Budgets in Indonesian Forests and Oil Palm Plantations, *Frontiers in Environmental Science*, 9, 48, <https://doi.org/10.3389/fenvs.2021.617828>, 2021.
- 580 United Nations Environment Programme (UNEP). Resolution 4/16. Conservation and Sustainable Management of Peatlands - Resolution Adopted by the United Nations Environment Assembly on 15 March 2019. <https://wedocs.unep.org/20.500.11822/30675>, 2019.

- Virkkala, A. M., Natali, S. M., Rogers, B. M., Watts, J. D., Savage, K., Connon, S. J., Mauritz, M., Schuur, E. A. G., Peter, D., Minions, C., Nojeim, J., Commane, R., Emmerton, C. A., Goeckede, M., Helbig, M., Holl, D., Iwata, H., Kobayashi, H.,  
585 Kolari, P., López-Blanco, E., Marushchak, M. E., Mastepanov, M., Merbold, L., Parmentier, F. J. W., Peichl, M., Sachs, T.,  
Sonnentag, O., Ueyama, M., Voigt, C., Aurela, M., Boike, J., Celis, G., Chae, N., Christensen, T. R., Bret-Harte, M. S., Dengel,  
S., Dolman, H., Edgar, C. W., Elberling, B., Euskirchen, E., Grelle, A., Hatakka, J., Humphreys, E., Järveoja, J., Kotani, A.,  
Kutzbach, L., Laurila, T., Lohila, A., Mammarella, I., Matsuura, Y., Meyer, G., Nilsson, M. B., Oberbauer, S. F., Park, S. J.,  
Petrov, R., Prokushkin, A. S., Schulze, C., St. Louis, V. L., Tuittila, E. S., Tuovinen, J. P., Quinton, W., Varlagin, A., Zona,  
590 D., and Zyryanov, V. I.: The ABCflux database: Arctic-boreal CO<sub>2</sub> flux observations and ancillary information aggregated to  
monthly time steps across terrestrial ecosystems, *Earth Syst Sci Data*, 14, 179–208, <https://doi.org/10.5194/ESSD-14-179-2022>, 2022.
- Werner, R. A., Buchmann, N., Siegwolf, R. T. W., Kornel, B. E., and Gessler, A.: Metabolic fluxes, carbon isotope  
fractionation and respiration – lessons to be learned from plant biochemistry, *New Phytologist*, 191, 10–15,  
595 <https://doi.org/10.1111/J.1469-8137.2011.03741.X>, 2011.
- Wright, E. L., Black, C. R., Turner, B. L., and Sjögersten, S.: Environmental controls of temporal and spatial variability in  
CO<sub>2</sub> and CH<sub>4</sub> fluxes in a neotropical peatland, *Global Change Biology*, 19, 3775–3789, <https://doi.org/10.1111/GCB.12330>,  
2013.
- Yu, Z., Beilman, D. W., Frohling, S., MacDonald, G. M., Roulet, N. T., Camill, P., and Charman, D. J.: Peatlands and Their  
600 Role in the Global Carbon Cycle, *Eos*, 92, 97–98, <https://doi.org/10.1029/2011EO120001>, 2011.